International Journal on Recent and Innovation Trends in Computing and Communication
ISSN: 2321-8169 Volume: 11 Issue: 5
DOI: https://doi.org/10.17762/ijritcc.v11i5.6603
***Article Received**: 24 February 2023 **Revised**: 30 March 2023 **Accepted**: 14 April 2023*

An Image Quality Selection and Effective Denoising on Retinal Images Using Hybrid Approaches

[*1]Binju Saju, [2]Rajesh R
[*1]Research Scholar, Department of Computer Science,
Christ (Deemed to be University), Bengaluru, Karnataka 560029, India.
Email: binju.saju@res.christuniversity.in
[2]Associate Professor, Department of Computer Science,
Christ (Deemed to be University), Bengaluru, Karnataka 560029, India.
Email: r.rajesh@christuniversity.in

Abstract: Retinal image analysis has remained an essential topic of research in the last decades. Several algorithms and techniques have been developed for the analysis of retinal images. Most of these techniques use benchmark retinal image datasets to evaluate performance without first exploring the quality of the retinal image. Hence, the performance metrics evaluated by these approaches are uncertain. In this paper, the quality of the images is selected by utilizing the hybrid naturalness image quality evaluator and the perception-based image quality evaluator (hybrid NIQE-PIQE) approach. Here, the raw input image quality score is evaluated using the Hybrid NIQE-PIQE approach. Based on the quality score value, the deep learning convolutional neural network (DCNN) categorizes the images into low quality, medium quality and high quality images. Then the selected quality images are again pre-processed to remove the noise present in the images. The individual green channel (G-channel) is extracted from the selected quality RGB images for noise filtering. Moreover, hybrid modified histogram equalization and homomorphic filtering (Hybrid G-MHE-HF) are utilized for enhanced noise filtering. The implementation of proposed scheme is implemented on MATLAB 2021a. The performance of the implemented method is compared with the other approaches to the accuracy, sensitivity, specificity, precision and F-score on DRIMDB and DRIVE datasets. The proposed scheme's accuracy is 0.9774, sensitivity is 0.9562, precision is 0.99, specificity is 0.99, and F-measure is 0.9776 on the DRIMDB dataset, respectively.

Keywords: Retinal Image, Image Quality, Quality Score, Pre-Processing, Noise Filtering, Green Channel.

I. INTRODUCTION

Eye vision is a necessary sense for all people. The retina is a thin membrane, the innermost layer of the eyeball. However, in the world, many people are suffering from vision impairments [1]. According to World Health Organization (WHO), in a 2017 report, 283 million people suffer from vision problems worldwide. Among them, 245 million people have a moderate impairment, and 38 million are blind. As per the international agency for the prevention of blindness (IAPB) 2017 report, over 7.4 billion worldwide, 253 million people are suffering from vision impairments, of which 37 million are blind, and 216 million have moderate vision problems [2]. Diabetics Retinopathy (DR) is one of the most problems of the patient with diabetics, and in the starting stage, DR has no pain and does not have any effect on the eye. DR rapidly causes severe vision problems and blindness when it is not treated properly. Detecting in early-stage and suitable treatment of DR can recover vision loss [3]. The WHO suggests periodic screening for people at high risk. Still, the low rate of ophthalmologists would force the manual screening of many people who need screening, particularly in developing countries and rural areas [4]. Automatic screening can overcome these drawbacks by offering easy capture and verifying patient images [5]. Retinal images are mainly exploited in DR automatic screening models as they have merits like non-invasive and cost-effective [6]. The diagnosis of DR includes blood vessels, optic disc and the macula segment [7].

Better quality retinal images should be provided for the automatic screening. These images can be degraded due to various factors like retina's curved structure, patient movement and camera settings [8]. Due to these reasons, a misdiagnosis could happen when early disease signs are concealed because of the image's poor quality, leading to delayed treatment. Retinal image quality assessment (RIQA) is important to guarantee that the images utilized for medical analysis are of sufficient quality for diagnosis [9]. RIQA methods generally consider the retinal images, which the medical experts manually explain as bad or good quality images. These images are used for training the classifier for differentiating bad and good quality retinal images [10]. The RIQA algorithm can be divided into two groups: histogram and segment-based IQA methods. In both methods, the image quality is found by the variation among its histogram and mean histogram of the good quality images. Many researchers are working on automatic RIQA using several methods [11]. The RIQA methods are grouped into three segments, namely (a) generic quality of image indicators, (b) structure of retinal images (c) both structure of retinal images and generic quality of image indicators [12]. The methods that use the generic quality of the

International Journal on Recent and Innovation Trends in Computing and Communication
ISSN: 2321-8169 Volume: 11 Issue: 5
DOI: https://doi.org/10.17762/ijritcc.v11i5.6603
***Article Received**: 24 February 2023 **Revised**: 30 March 2023 **Accepted**: 14 April 2023*

image do not segment the image and consume only low computational power [13].

The existing machine learning (ML) techniques are based on expert people for the relevant handcrafter features extraction. Deep learning (DL) [14] models learn the high-level features from the data without the need of the expert people. Thus, the DL methods have been gaining popularity in the medical field application [15]. Convolutional Neural Network (CNN) is the popular DL exploited in computer vision processes like classification of images and object detection. CNN is trained for extracting features from images [16]. The extension of CNN is DCNN which generates new images by the extracted features [17]. This article mainly focuses on the pre-processing technique, improving image quality. After selecting image quality, image filtering techniques should be applied to remove the noise. There are problems accompanied by retinal images, which analyze retinal complex, and these issues occur due to noise in the image. Many approaches have been developed to improve the contrast and remove noise. In this article, the contract of the image is improved by a Modified histogram equalizer (MHE), and the noise is removed by homomorphic filtering [18] [19] [20].

Motivation: Detecting the retinal images manually is labour-intensive and takes more time to process. Therefore, Computer Assisted Diagnostic (CAD) has been used recently for image analysis. This automated RIQA can minimize the requirement for human intervention, low cost, and offer good services in remote places. RIQA is a necessary precondition for retinal disease detection. Its motive is to find retinal images in which the structure of anatomic and lesions attracts the attention of ophthalmologists. Most images are displayed clearly and reject the poor quality retinal images. The success of these automated systems relies on image quality. But due to the various lighting and movement of the patient, the images will be blurred with noise and affect the detection accuracy. Over the last two decades, numerous approaches have been developed, combining various automatic retinal image analysis methods. Recently, DL approaches that hybrid multi-level representations have been developed for obtaining remarkable performances in medical imaging analysis. Different from the existing model, DL can determine the hidden information in the original feature, which improves the robustness of the model.

Contributions

- The pre-processing is the major part of this work. Here, the raw input image quality score is evaluated using the Hybrid NIQE-PIQE approach.
- Based on the quality score value DCNN categorizes the images into low quality, medium quality and high-quality images.
- Then the selected quality images are again pre-processed to remove the noise present in the images. The individual G-channel is extracted from the selected quality RGB images.
- Hybrid G-MHE-HF is utilized for contrast enhancement and noise removal.
- The performance of the implemented method is compared with the other approaches with respect to accuracy, sensitivity, specificity, precision, and F-measure.

The remaining structure of the research article is arranged as follows: section 2 gives the recent related research works; section 3 explains the developed scheme; section 4 gives the discussion of implemented results; and last, section 5 gives the overall conclusion.

II. RELATED WORKS

Some of the recently introduced techniques in RIQA using different models are listed below:

Coyner et al. [21] analyzed the quality of an image in retinopathy of prematurity (ROP) using DCNN. The retinal fundus images were gathered from premature babies on ROP screening. Totally, 6139 images were gathered from nine institutions. The images were grouped based on their quality. The 5-fold cross fold was used to avoid overfitting problems and for estimating the test performance. The performance of the CNN was implemented by the receiver operating characteristic curve (ROC). Further, this model can be applied in telemedicine and clinical setting.

TABLE 1 Features and challenges of the existing models

Authors and citations	Methods	Features	Challenges
Coyner *et al.* [21]	DCNN	Reduces the overfitting problem Exactly determine the high and low quality images	This model was restricted only to RetCam images and did not support other images. It was unclear whether this method could classify the images gathered from adults.
Chalakkal *et al.* [22]	DCNN	Achieves better classification and convergence speed is faster	The implementation cost was high

International Journal on Recent and Innovation Trends in Computing and Communication
ISSN: 2321-8169 Volume: 11 Issue: 5
DOI: https://doi.org/10.17762/ijritcc.v11i5.6603
***Article Received**: 24 February 2023 **Revised**: 30 March 2023 **Accepted**: 14 April 2023*

Abdel-Hamid and Lamiaa [23]	VGG 16 with TL	Achieved better accuracy	This model does not support images from other sources
Pratap *et al.* [24]	CNN with SVM	Achieved better testing and training accuracy	This method was prone to overfitting problem
Sun *et al.* [25]	CNN	Achieved better accuracy and ROC of about 97.1% and 0.9%	This model takes more time for the training process

Chalakkal et al. [22] presented a DL-based RIQA implementation method. The classification of level 1 was based on the DL method, and level 2 was based on unsupervised learning. The level 1 classifier analyzed the retinal images, and the level 2 classifier analyzed the field definition. With the help of these two classifiers, the images were classified into high and low quality images. This model was more robust, and it was suitable for medical practice.

Abdel-Hamid and Lamiaa [23] used a modified VGG 16 architecture and transfer learning (TL) for classifying the retinal images in RIQA analysis. The wavelet details and spatial are inputs given to the VGG architecture because it has the relevant data based on the retinal image quality. The experimental results were carried out on the different datasets, and the experiments were done with and without TL. Finally, this model achieved higher accuracy and performed well compared to other RIQA methods.

Pratap et al. [24] presented a method for cataract diagnosis, which has several stages like normal, mild, moderate and severe, using the fundus images. This model utilized the pre-trained CNN for the TL to classify cataracts. Further, pre-trained CNN was used to extract features, which were given to the Support Vector Machine (SVM). The image selection quality was used when the quality level was not matched with the testing and training. The model achieved an accuracy of about 92.91%. This model was more helpful for the people living in rural areas.

Sun et al. [25] evaluated the various CNN (VGG-16, ResNet-50, AlexNet and GoogLeNet) performances in the classification of retinal images. This model evaluated the two major factors, namely pre-processing and data augmentation. These two factors were important in the application of medical images. It was proved that the GoogLeNet fine-tuned using ImageNet has a better pre-processing of the image, and data augmentation achieved a better accuracy in the traditional CNN architectures. Moreover, the classification result from a natural image can still transfer to make medical image quality classification efficiently. Table 1 represents the Features and challenges of the existing models

III. PROPOSED METHODOLOGY

This section explains the methodology of image quality selection, pre-processing and noise removal in the image. A hybrid RIQA technique is developed based on image quality. This paper mainly focused on pre-processing technique. The process of image quality is explained in detail in the below sections.

Figure 1 shows the schematic diagram of the implemented scheme. Here, the raw input image quality score is evaluated using the Hybrid NIQE-PIQE approach. Based on the quality score value DCNN categorizes the images into low quality, medium quality and high quality images. Then the selected quality images are again pre-processed to remove the noise present in the images. The individual G-channel is extracted from the selected quality RGB images. Hybrid G-MHE-HF is utilized for contrast enhancement and noise removal.

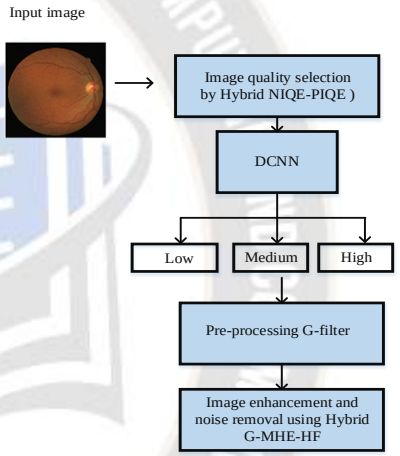

Figure 1 Schematic diagram of the implemented scheme

A) Hybrid NIQE-PIQE for Retinal image score selection

In the DL algorithm, image quality plays a major role. In this work, the quality of the image selection is added to filter out the good quality retinal image for further detection. The image quality is estimated by a no-reference image quality evaluator hybrid NIQE-PIQE. This hybrid model provides fewer scores for good images, and poor images achieve high scores. The trained regression model performance is based on the training database selection, which requires ground-truth subjective option scores. Inspired by the model completely blind NIQE and also trained pristine multivariate Gaussian (MVG) method form high quality retinal image collection. The natural scene statistics (NSS) calculated from the natural image can be achieved by attaching them with the density of MVG, and it can be represented as:

$$f_Y(y_1, y_2 \ldots\ldots, y_l) = \frac{1}{(2\pi)^{l/2} |\sum|^{1/2}} e\left(-\frac{1}{2}(y-u)^t \sum^{-1} (y-u)\right) \quad (1)$$

International Journal on Recent and Innovation Trends in Computing and Communication
ISSN: 2321-8169 Volume: 11 Issue: 5
DOI: https://doi.org/10.17762/ijritcc.v11i5.6603
***Article Received**: 24 February 2023 **Revised**: 30 March 2023 **Accepted**: 14 April 2023*

Where $f_Y(y_1, y_2.....,y_l)$ is the feature of NSS, u and $\sum$ are the mean and covariance of the MVG. Then the retinal images are divided into k patches $p \times p$. By calculating the features of NSS, every patch attached by MVG is defined by $(u_j, \sum_j)$, and MVG $(u, \sum)$ is calculated for driving a local quality score. The distorted image quality is the distance between MVG attached to the feature and NSS, and it is given by

$$d = \sqrt{(u_1 - u_2)^t \left(\frac{\sum_a + \sum_b}{2} \right)^{-1} (u_1 - u_2)} \quad (2)$$

Where u_1 and u_2 are the mean, $\sum_a, \sum_b$ are the covariance of natural MVG and distorted MVG.

But, NIQE utilizes a single global MVG technique for describing the image, and use local image information, which is used for predicting the image quality, is lost. Therefore the model is a hybrid with PIQE.

PIQE involves features of NSS extracted from luminance image given by

$$\overset{\Delta}{I}(k,l) = \frac{I(k,l) - u(k,l)}{\sigma(k,l) + K} \quad (3)$$

Where u and σ are mean and variance. $k = \{1,.....,M\}$, $l = \{1,.....,N\}$, M and N are the height and width of the image and K is constant. The input image is segmented into non-overlapping blocks, and the Mean Subtracted Contrast Normalized (MSCN) coefficients are used for labelling a block by uniform block (U) or non-uniform block (NU), which is expressed as

$$b_k = \begin{cases} U & u_k < t_U \\ NU & u_k < t_U \end{cases} \quad (4)$$

Where u_k is an MSCN variance, $\overset{\Delta}{I}(k,l)$ in a block, b_k, $k = \{1,.....,n_B\}$, n_B is the total block of size $n \times n$.

The segment undergoes less spatial activity, if the standard deviation σ of the structural element is less than the threshold value T.

$$\sigma < T \quad (5)$$

Additional perception based centre surround criterion is considered here to model noise distortion using block level MSCN features. This criterion is inspired by the Human Visual System's (HVS) sensitivity to centre surround variations. The relation is given by

$$\gamma = \frac{\left| \left(\frac{\sigma_c}{\sigma_s} \right) - \sigma_{bk} \right|}{\max\left(\frac{\sigma_c}{\sigma_s} \right), \sigma_{bk})} \quad (6)$$

Where σ_c and σ_s are the segment standard deviation, σ_{bk} is a standard deviation of the non-uniform block. If the SNR is high, γ is equal to σ_{bk}. Hence a given block can be classified as affected noise when it satisfies the condition

$$\sigma_{bk} > 2 \times \gamma \quad (7)$$

Let v_{bk} is the variance feature for assigning the distortion amount for a distorted block, and the distortion procedure is given by

$$d_{bk} = \begin{cases} 1 & if\,(5) and (7) \\ v_{bk} & if\,(7) \\ (1 - v_{bk}) & if\,(5) \end{cases} \quad (8)$$

Perception based Image Quality Evaluator, PIQE is expressed as

$$PIQE = \frac{\left(\sum_{k=1}^{N_{NU}} d_{bk} \right) + K_1}{(N_{Nu} + K_1)} \quad (9)$$

B) DCNN for image quality selection

After selecting the score, the DCNN is used to classify the good, medium and poor quality images. DCNN has a convolutional layer, pooling layer, and fully connected layer.

International Journal on Recent and Innovation Trends in Computing and Communication
ISSN: 2321-8169 Volume: 11 Issue: 5
DOI: https://doi.org/10.17762/ijritcc.v11i5.6603
***Article Received**: 24 February 2023 **Revised**: 30 March 2023 **Accepted**: 14 April 2023*

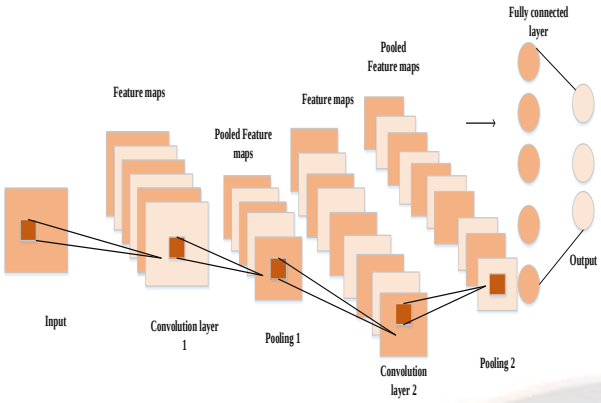

Figure 2 Architecture of DCNN

Figure 2 shows the architecture of DCNN. The convolutional layer consists of a set of filters used to extract the local features from the input. Each filter is used to calculate feature maps. The pooling layer minimizes the feature maps solution. Pooling generates invariance to a small distortion. Fully connected layers (FC) have neurons and filters where the levels of high reasoning are carried out. Here the computations are done by matrix multiplication and bias offset. The layers of the DCNN are explained below.

Convolutional layer: Let the convolutional layer be CL and the feature maps ${f_1}^{(CL-1)}$ of size ${f_2}^{(CL-1)} \times {f_3}^{(CL-1)}$. ${X_j}^{CL}$ is a j^{th} feature map in the layer CL and it is expressed in the following equation.

$$X_j^{CL} = e_j^{CL} + \sum_{i=1}^{f_1^{(CL-1)}} J_{j,i}^{(CL)} * X_i^{(CL-1)} \quad (10)$$

Where e_j^{CL} is the bias matrix, for $2_{u1}^{CL}+1 \times 2_{u2}^{CL}+1$ is the filter size accomplishing the i^{th} feature map in the layer $(CL-1)$ with the feature map in the layer CL is $J_{j,i}^{(CL)}$ and $X_i^{(CL-1)}$ is a network trainable weight? The size of the output feature map is given by

$${f_2}^{CL} = {f_2}^{(CL-1)} - 2u_1^{CL} \text{ And } {f_3}^{CL} = {f_3}^{(CL-1)} - 2u_2^{CL} \quad (11)$$

Finally, the filter that is exploited for the calculation of the constant feature map ${X_j}^{CL}$ are same. That is $J_{j,i}^{(CL)} = J_{j,k}^{(CL)}$ for $i \neq k$. In the layer CL, all feature maps the ${X_j}^{CL}$ has ${f_2}^{CL}.{f_3}^{CL}$ organized in 2D array form. At the position (m,n), the output is calculated by

$$(X_j^{CL})_{g,b} = (e_j^{CL})_{m,n} + \sum_{i=1}^{f_1^{(CL-1)}} (J_{j,i}^{(CL)} * X_i^{(CL-1)})_{m,n} \quad (12)$$

$$= (e_j^{CL})_{m,n} + \sum_{i=1}^{f_1^{(CL-1)}} \sum_{c=-u_1^{CL}}^{u_1^{CL}} \sum_{c=-u_2^{CL}}^{u_2^{CL}} (J_{j,i}^{(CL)})_{c,d} * X_i^{(CL-1)})_{m+c,n+d} \quad (13)$$

Non-linearity layer: Let us assume the layer CL as a Non-linearity layer, where the input ${f_1}^{CL}$ output and feature maps are comprised with ${f_1}^{CL} = {f_1}^{(CL-1)}$) is given as follows

$$X_j^{CL} = F(X_j^{(CL-1)}) \quad (14)$$

Here F is the function of activation, and the coefficient of the gain is given by

$$X_j^{CL} = mB_j F(X_j^{(CL-1)}) \quad (15)$$

Rectification: In rectification, the exact value for the feature map is calculated by the following equation, and here the exact value evaluation is developed pointwise. Therefore, the output has ${f_1}^{CL} = {f_1}^{(CL-1)}$) a feature map not modified in size.

$$X_j^{CL} = | X_j^{CL} | \quad (16)$$

Local contrast normalization layer: The Local contrast normalization layer aims to establish the local competitiveness between feature maps adjacent units and spatial location units. The subtractive normalization operation output of the CL is calculated by the following Equations.

$$X_j^{CL} = X_j^{(CL-1)} - \sum_{i=1}^{f^{(CL-1)}} JP(\sigma) * X_j^{(CL-1)} \quad (17)$$

$$(X_j^{CL})_{m,n} = \frac{(X_j^{(CL-1)})_{m,n}}{\left(R + \mu \sum_{i=1}^{f_1^{(CL-1)}} (X_j^{(CL-1)})_{m,n}^2\right)^{\mu}} \quad (18)$$

Where R and μ are the hyperparameters.

Feature pooling and subsampling layer: Basically, in each feature map, the pooling creates using locating window at the position of non-overlapping and keeps one value for each

International Journal on Recent and Innovation Trends in Computing and Communication
ISSN: 2321-8169 Volume: 11 Issue: 5
DOI: https://doi.org/10.17762/ijritcc.v11i5.6603
Article Received: 24 February 2023 Revised: 30 March 2023 Accepted: 14 April 2023

window. Therefore, feature map subsampling is developed. The two types of pooling layers are average pooling and max pooling layers.

Fully connected layer: When the layer CL is not fully connected, then the feature maps $f_1^{(CL-1)}$ of size $f_2^{(CL-1)} \times f_3^{(CL-1)}$ is considered as input and i^{th} layer with j^{th} is expressed as

$$f_j^{CL} = f(v_i^{CL}) \; with \; v_i^{CL} = \sum_{i=1}^{f_1^{CL-1}} \sum_{m=1}^{f_2^{CL-1}} \sum_{n=1}^{f_3^{CL-1}} wt_{i,j,m,n}^{CL} (X_i^{(CL-1)} \quad (19)$$

Where $wt_{i,j,m,n}^{CL}$ is the weight associated with the position (m,n).

C) Pre-processing

In a pre-processing step, the G-channel is extracted from the RGB retinal image, and it is mainly used pre-processing method in the computerized diagnosis of retinal detection. The merits of the G-channel are given as follows.

- The G-channel has the contrast feature among the background and object. In addition, the illumination is poor for green and red channels.
- The extraction of the G-channel is simple and efficient
- The time of processing is reduced by one-third of the original time

So the G-channel is extensively utilized for improving non-uniform retinal image illumination.

D) Noise removal by Hybrid G-MHE-HF

The performance of the proposed method with the input G-channel and histogram equalization of the input G-channel is evaluated. The histogram equalization is a good technique to improve the luminance conditions of an image

An image's histogram is a pictorial indication of the relative frequency of an image's various gray levels. Many contrast enhancement approaches based on the histogram are available for improving the visible image quality. One of the common methods is Histogram equalization (HE). HE is a pre-processing method that improves contrast for all kinds of images. Equalization suggests mapping from given intensity distribution to uniform intensity distribution. Therefore, the intensity values are developing in the whole range and can obtain close to equally distributed intensities in an output image.

Let us consider the image as a two dimensional gray level array in HE. If the (j,k) element of the array is $Y(j;k)$ is the intensity of (j,k) image pixel where $Y(j;k)$ is from the D discrete gray levels represented as $\{Y_0, Y_1 ..... Y_{D-1}\}$. The Probability Mass Function (PMF) of a gray level Y_i is indicated as $P[Y_i]$ and it stated as:

$$P[Y_i] = \frac{m_i}{m} \text{ Where } k = 0,1....D-1 \quad (20)$$

Where m_i is the number of the pixel with intensity k and m is the overall pixel in an image.

Let the cumulative distribution function (CDF) of Y_i is represented as $C[Y_i]$ and it is expressed as

$$C[Y_i] = P[Y \le y] = \sum_{j=0}^{k} \frac{m_i}{m} \text{ Where } k = 0,1...D-1 \quad (21)$$

It is clear that the $C[Y_{D-1}] = 1$. Then for HE, a transform function is $F(.)$ which maps a gray level of input Y_i into a gray level of output $F(i)$ is represented as

$$F(Y_i) = Y_0 + (Y_{D-1} - Y_0)\, C[Y_i] \text{ Where } k = 0,1...D-1 \quad (22)$$

E) Hybrid MHE-HF

There are two pre-processing stages: in the first stage, MHE improves global image contrast, and in the second stage, HF is exploited for image sharpening and normalization of image. The limitation of HE is that it does not offer a mechanism which could adjust the enhancement level. Here MHE is introduced for contrast enhancement. This modified model can control the contrast enhancement level in an output image.

Let H be the histogram's input image and H_u is the uniform histogram. Then the modified histogram equalization is expressed as

$$H_m = \gamma H_u + (1-\gamma) H \text{ Where } 0 \le \gamma \le 1 \quad (23)$$

In this work $\gamma = 0.55$ is considered.

Basically, contrast enhancement also has noise enhancement; therefore, HF is applied to reduce the noise content in a HE image. HF is a popular approach for enhancing and restoring degraded images with unequal illumination. This method utilizes the illumination reflectance method in its operation. Two components characterize this approach. One is

International Journal on Recent and Innovation Trends in Computing and Communication
ISSN: 2321-8169 Volume: 11 Issue: 5
DOI: https://doi.org/10.17762/ijritcc.v11i5.6603
***Article Received**: 24 February 2023 **Revised**: 30 March 2023 **Accepted**: 14 April 2023*

the incidence component, and the second one is reflectance. An image $f(x_i, y_i)$ is stated as:

$$f(x_i, y_i) = i(x_i, y_i) r(x_i, y_i) \tag{24}$$

Where $i(x_i, y_i)$ and $r(x_i, y_i)$ are the incidence and reflected components.

Here, the intensity of incidence is slower than the intensity of reflectance. Hence $r(x_i, y_i)$ is considered a high frequency component than $i(x_i, y_i)$. Considering this fact, the HF method aims to reduce the significance of $i(x_i, y_i)$ by minimizing the low frequency component of an image. Filtering techniques in the frequency domain can demonstrate this. To do this image has to transform to a frequency domain from a special domain. This can be demonstrated by Fourier transforms. Then applying HF, normalization of the image is applied, and it is expressed as:

$$g(x_i, y_i) = \left(\frac{Y_{MI}}{Y_{MO}} \right) f(x_i, y_i) \tag{25}$$

Where Y_{MI} aninput image is mean brightness and Y_{MO} is the image generated after HF, respectively.

IV. RESULT AND DISCUSSION

This section gives the performance analysis and discussion of the image quality selection of the proposed scheme. The entire implementation has been processed on a system with 8 GB RAM and an Intel Core i5 CPU with 3.0 GHz speed. To implement the proposed scheme, MATLAB 2021a is utilized. The performance of the proposed method is compared with the Gaussian and Bilateral filters.

F) Dataset Details

Diabetic Retinopathy Images Database (DRIMDB): DRIMDB dataset was developed by Sevik *et al.* This dataset has 216 images got from the Retina Department of Ophthalmology, Medical Faculty at Karadeniz Technical University in Turkey. Images were obtained by Canon camera and saved in JPEG format at 570x760 pixels. These images are categorized into 3 classes, namely 125 good images (MSRI), 69 bad images (not MSRI) and 22 outlier images (non-retinal).

Digital Retinal Images for Vessel Extraction (DRIVE) dataset: This database is used for retinal vessel segmentation. It has 40 fundus images of RGB in JPEG format, and a green channel is considered for our implementation. It also has seven abnormal pathology images. The images were received from a diabetic retinopathy screening program in the Netherlands and obtained by a Canon camera. The resolution of every image is 584*565 pixels with 8 bits per colour channel. Forty images were equally split into testing and training (20 images). An ophthalmological expert has applied one manual segmentation for each image within the training set. Similarly, two manual segmentations for each image within the training set are given by two observers.

G) Performance Measures

To quantitatively calculate the developed scheme's performance, some metrics are commonly employed. The metrics with the formula are described below.

Accuracy: The accuracy measure determines the overall system's efficiency. For the proposed technique, accuracy is the ratio of exactly identified pixels

$$A = \frac{T_p + T_n}{T_p + T_n + F_p + F_n} \tag{26}$$

***Sensitivity**:* It computes the positive proportions that are exactly determined. The formulation of sensitivity measure can be depicted as follows:

$$Se = \frac{T_p}{T_p + F_n} \tag{27}$$

Specificity: It computes the negative proportions that are exactly determined. The formulation of sensitivity measure can be depicted as follows:

$$Sp = \frac{T_n}{T_n + F_p} \tag{28}$$

F1-score: The ensemble mean of sensitivity and precision.

$$F1 - score = \frac{2T_p}{2T_p + F_p + F_n} \tag{29}$$

Precision: The proportion of predicted positives which are genuine positives.

$$P = \frac{T_p}{T_p + F_p} \tag{30}$$

Where T_p, F_p, F_n and T_n are accurately identified pixel, incorrectly identified pixel, incorrectly identified pixel background pixel and accurately identified non-pixel

Mean Squared Error (MSE): The average squared variation among the actual and estimated values is expressed as

$$MSE(a,b) = \frac{1}{n} \sum_{i=1}^{n} (a_i - b_i)^2 \tag{31}$$

Peak Signal to Noise Ratio (PSNR): The ratio between the maximum possible power of a signal and the power of corrupting noise affects the fidelity of its representation.

International Journal on Recent and Innovation Trends in Computing and Communication
ISSN: 2321-8169 Volume: 11 Issue: 5
DOI: https://doi.org/10.17762/ijritcc.v11i5.6603
Article Received: 24 February 2023 Revised: 30 March 2023 Accepted: 14 April 2023

$$PSNR = 10\log_{10}\frac{P^2}{MSE} \quad (32)$$

Where P is the pixel intensities dynamic range.

Structural Similarity Index (SSIM): SSIM is used to calculate the similarity between two images, and it is expressed as

$$SSIM = [I(a,b)]^{\alpha},[c(a,b)]^{\beta},[s(a,b)]^{\gamma} \quad (33)$$

H) Performance on DRIVE dataset

This section shows the performance based on the DRIVE dataset. The results are implemented for good images. Then the images are divided according to the score values. Here a low score is given for the good quality images, a high score is given for the bad quality, and a medium score is given for the medium quality images.

Figure 3 depicts the colour fundus as an RGB with 3 channels which shows several retina structures. For pre-processing green channel is chosen for the further process because it gives the highest contrast between the background and image. G- Channel has much visibility when compared to the other two channels. The fundus camera takes images at various FOVs needed for superimposing the non-retinal image part.

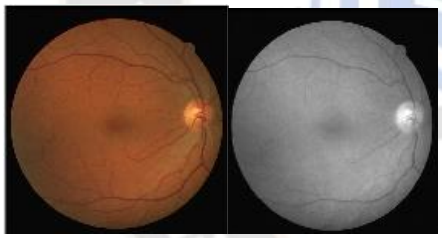

(a) (b)

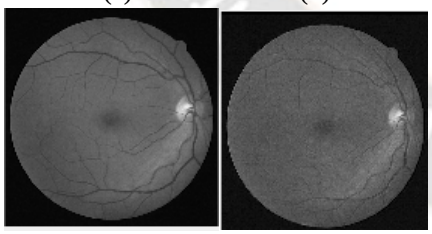

(c) (d)

Figure 3 Fundus image of RGB (a) input image (b) red channel (c) Green channel (d) Blue channel

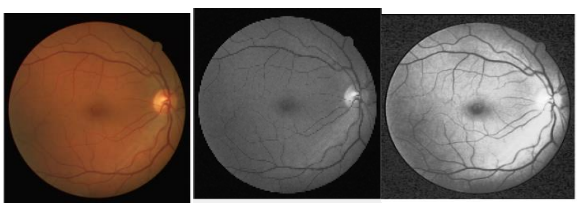

(a) (b) (c)

(d)

Figure 4 Image quality Detection of various methods (a) input image (b) Green channel (c) modified HE (d) proposed

Figure 4 shows the image quality detection of various methods. The overall implementation of the proposed scheme is shown in figure 3. Figures (a) and (b) show the input and green channel images. Figure (c) shows the modified HE image is developed to reduce the noise, but noise is still present in the image. To tackle this problem and improve the image contrast our proposed scheme is employed which provides the image with better quality and is shown in Figure (d).

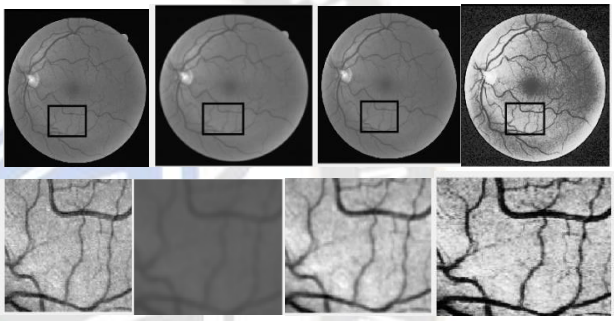

(a) (b) (c) (d)

Figure 5 Comparison of image denoising (a) input (b) Gaussian Filter (c) Bilateral filter (d) proposed method

Figure 5 shows the comparison of image denoising (a) input (b) Gaussian Filter (c) Bilateral filter (d) proposed method. Here the above image represents the original image denoised by several methods. The below image is an enlarged view of an image. From the result, we can observe that the Gaussian filter produces blur image and the bilateral filter performs well, but when compared to the proposed scheme, it provides a low image contrast. Finally, our proposed scheme provides a better image with a denoised image. Hence, the proposed filter produces superior results compared to the other two filters.

International Journal on Recent and Innovation Trends in Computing and Communication
ISSN: 2321-8169 Volume: 11 Issue: 5
DOI: https://doi.org/10.17762/ijritcc.v11i5.6603
***Article Received**: 24 February 2023 **Revised**: 30 March 2023 **Accepted**: 14 April 2023*

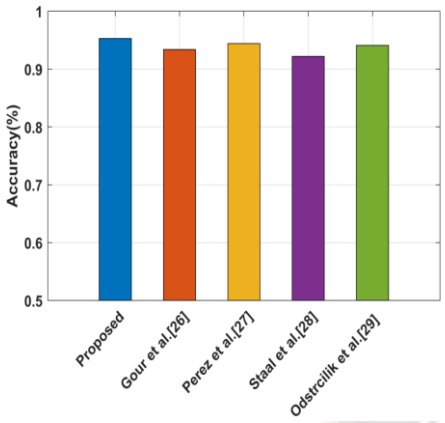

Figure 6 Accuracy comparison of the various approaches

Figure 6 shows the Accuracy comparison of the various approaches for the DRIVE dataset. Here the accuracy of the method proposed by Gour et al. [26] is 0.94, Perez et al. [27] is 0.922, Staal et al. [28] is 0.944, and Odstrcilik et al. [29] are 0.934. Finally, our proposed method shows higher accuracy of about 0.955. Thus the proposed method showed its betterment by accuracy.

Figure 7 shows the sensitivity comparison of the various approaches for the DRIVE dataset. Here the sensitivity of the method proposed by Gour et al. [26] is 0.721, Perez et al. [27] is 0.66, Staal et al. [28] is 0.71, and Odstrcilik et al. [29] is 0.70. Finally, our proposed method shows higher sensitivity of about 0.80. Thus the proposed method showed its betterment by sensitivity.

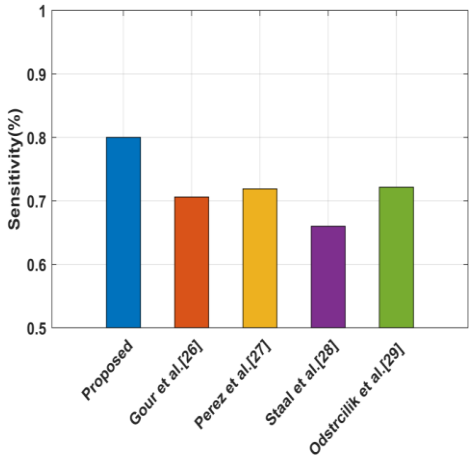

Figure 7 Sensitivity comparison of the various approaches

Figure 8 shows the specificity comparison of the various approaches for the DRIVE dataset. Here the specificity of the method proposed by Gour et al. [26] is 0.972, Perez et al. [27] is 0.962, Staal et al. [28] is 0.97, and Odstrcilik et al. [29] is 0.969. Finally, our proposed method shows higher specificity of about 0.977. Thus the proposed method showed its betterment by specificity.

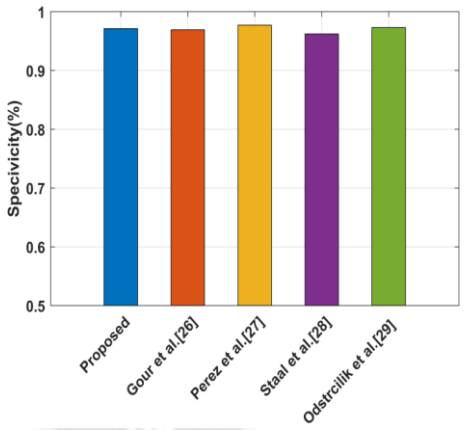

Figure 8 Specificity comparison of the various approaches

TABLE 2 Performance evaluation of DRIMDB Dataset

Methods	Accuracy	Specificity	Sensitivity	Precision	F1-score
Gaussian filter	0.9712	0.98	0.7615	0.9876	0.9744
Bilateral filter	0.9753	0.97	0.9746	0.9752	0.9749
Proposed	0.9774	0.99	0.9562	0.99	0.9776

Table 2 shows the performance evaluation of the DRIMDB Dataset. Here the performance of the proposed scheme is compared with the Gaussian and bilateral filters. It is seen that the proposed scheme attains a better accuracy of about 0.9774, while the bilateral and Gaussian filters attain an accuracy of about 0.9753. It is proved that in the DRIMDB dataset also proposed scheme has proved its betterment.

TABLE 3 Comparison of conventional and proposed filters

Filters	MSE	PSNR	SNR	SSIM
Gaussian filter [35]	0.002	26.35	21.6	0.59
Adaptive filter [35]	0.0009	30.3	25.6	0.80
Proposed (DRIVE dataset)	0.0216	64.79	56.789	0.99
Proposed (DRIMD Dataset)	0.0012	77.4391	77.0616	0.9920

Table 3 compares conventional and proposed filters to MSE, PSNR, SNR and SSIM values. The proposed scheme achieves better results in all cases than Gaussian and Adaptive filters. The PSNR value of the proposed method is 64.79, while for Gaussian and adaptive filters, the PSNR value is 26.35 and 30.3, respectively.

International Journal on Recent and Innovation Trends in Computing and Communication
ISSN: 2321-8169 Volume: 11 Issue: 5
DOI: https://doi.org/10.17762/ijritcc.v11i5.6603
***Article Received**: 24 February 2023 **Revised**: 30 March 2023 **Accepted**: 14 April 2023*

TABLE 4 Comparison of processing time on DRIVE dataset

Methods	Processing Time
Zhao et al. [30]	2 min
Cinsdikici et al. [31]	35 s
Roychowdhury et al. [32]	3.1 s
Fraz et al. [33]	2 min
Dash et al. [34]	1.6s
Proposed (DRIVE)	0.0822s
Proposed (DRIMDB)	0.0954s

Table 4 shows the comparison of processing time on the DRIVE dataset. Compared to other methods, the execution time of the proposed scheme is 0.0822s and 0.0954s on DRIVE and DRIMDB datasets, respectively. It is proved that the proposed scheme is time-efficient as it can execute the process within a short time.

Figure 9 represents the score values of the NIQE, PIQE and the hybrid NIQE-PIQE. The hybrid NIQE-PIQE acquire low score for good quality images and achieve high scores for poor quality images. The experimental analysis shows that the maximum values of hybrid NIQE-PIQE for good quality images are 12 and 28, respectively.

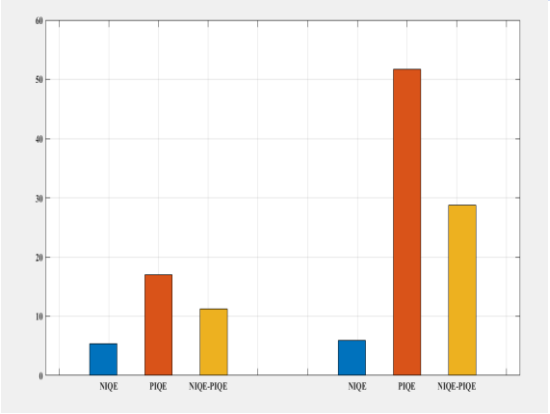

Figure 9 Comparison of score values of NIQE, PIQE and hybrid NIQE-PIQE

V. CONCLUSION

In this paper, the quality of the images is selected by utilizing the hybrid NIQE-PIQE) approach. Here, the raw input image quality score is evaluated using the Hybrid NIQE-PIQE approach. Based on the quality score value, DCNN categorizes the images into low quality, medium quality and high quality. Then the selected quality images are again pre-processed to remove the noise present in the images. The individual green channel (G-channel) is extracted from the selected quality RGB images for noise filtering. Moreover, Hybrid G-MHE-HF is utilized for enhanced noise filtering. The implementation of proposed scheme is implemented on MATLAB 2021a. The performance of the implemented method is compared with the other approaches with respect to certain metrics. The proposed scheme's accuracy is 0.9774, sensitivity is 0.9562, precision is 0.99, specificity is 0.99, and F-measure is 0.9776 on the DRIMDB dataset. Further, the execution time of the proposed scheme is 0.0822s and 0.0954s on DRIVE and DRIMDB datasets. Thus the proposed scheme showed its superiority in all the cases. In this work, pre-processing is only done to improve image quality. Future feature extraction and classification methods will be further included for better image quality.

ACKNOWLEDGMENT

None

REFERENCES

[1] R.V. Moiseev, P.W. Morrison, F. Steele, V.V. Khutoryanskiy, "Fraser Steele, and Vitaliy V. Khutoryanskiy. "Penetration enhancers in ocular drug delivery." *Pharmaceutics*, vol. 11, no. 7, pp. 321, 2019.

[2] R.R. Bourne, S.R. Flaxman, T. Braithwaite, M.V. Cicinelli, A. Das, J.B. Jonas, J. Keeffe, J.H. Kempen, J. Leasher, H. Limburg, K. Naidoo, "Magnitude, temporal trends, and projections of the global prevalence of blindness and distance and near vision impairment: a systematic review and meta-analysis", *The Lancet Global Health* vol. 5, no.9, pp. e888-e897, 2017.

[3] Mansour, S.E.; Browning, D.J.; Wong, K.; Flynn Jr, H.W.; Bhavsar, A.R. "The evolving treatment of diabetic retinopathy". *Clinical Ophthalmology (Auckland, NZ)*, vol. 14, pp. 653, 2020.

[4] A. Imran, J. Li, Y. Pei, J.J. Yang, Q. Wang, "Comparative analysis of vessel segmentation techniques in retinal images." *IEEE Access*, pp.114862-114887, vol. 7, 2019,

[5] B. Harangi, J. Toth, A. Baran, A. Hajdu, "Automatic screening of fundus images using a combination of convolutional neural network and hand-crafted features." *In 2019 41st Annual International Conference of the IEEE Engineering in Medicine and Biology Society (EMBC)*, pp. 2699-2702, 2019. IEEE.

[6] L. Abdel-Hamid, A. El-Rafei, G. Michelson, "Deep multiple instance learning for automatic detection of diabetic retinopathy in retinal images". *IET Image Processing*, vol. 12, no. 4, pp.563-571, 2018.

[7] S.N. Sangeethaa, P.U. Maheswari, "An intelligent model for blood vessel segmentation in diagnosing DR using CNN". *Journal of medical systems*, vol. 42, no. 10, pp.1-10, 2018.

[8] L. Abdel-Hamid, A. El-Rafei, G. Michelson, No-reference quality index for color retinal images'. *Computers in biology and medicine*, vol. 90, pp.68-75, 2017.

[9] H.Fu, B. Wang, J. Shen, S. Cui, Y. Xu, J. Liu, L. Shao, "Evaluation of retinal image quality assessment networks in different color-spaces." *In International Conference on Medical Image Computing and Computer-Assisted Intervention*, pp. 48-56, 2019. Springer, Cham.

[10] J. Lin, L. Yu, Q. Weng, X. Zheng, "Retinal image quality assessment for diabetic retinopathy screening: A survey." *Multimedia Tools and Applications*, pp. 1-27, 2019.

International Journal on Recent and Innovation Trends in Computing and Communication
ISSN: 2321-8169 Volume: 11 Issue: 5
DOI: https://doi.org/10.17762/ijritcc.v11i5.6603
***Article Received**: 24 February 2023 **Revised**: 30 March 2023 **Accepted**: 14 April 2023*

[11] L. Abdel-Hamid, A. El-Rafei, S. El-Ramly, G. Michelson, "Performance dependency of retinal image quality assessment algorithms on image resolution: analyses and solutions." Signal, *Image and Video Processing*, vol. 12, no. 1, pp.9-16, 2018.

[12] G.T. Zago, R.V. Andreão, B. Dorizzi, E.O.T. Salles, "Retinal image quality assessment using deep learning." *Computers in biology and medicine*, vol. 103, pp. 64-70, 2018.

[13] Y.P. Liu, Y. Lv, Z. Li, J. Li, Y. Liu, P. Chen, R. Liang, "Blood vessel and background separation for retinal image quality assessment." *IET Image Processing*, 2021.

[14] M. Islam, T.N. Poly, B.A. Walther, H.C. Yang, Y.C.J. Li, "Artificial intelligence in ophthalmology: a meta-analysis of deep learning models for retinal vessels segmentation". *Journal of clinical medicine*, vol. 9, no. 4, pp.1018, 2020.

[15] S.M. Muddamsetty, T.B. Moeslund, "Multi-level quality assessment of retinal fundus images using deep convolution neural networks." *In 16th International Joint Conference on Computer Vision Theory and Applications (VISAPP-2021) SCITEPRESS Digital Library*, 2020.

[16] L. Nanni, S. Ghidoni, S. Brahnam, "Handcrafted vs. non-handcrafted features for computer vision classification." *Pattern Recognition*, vol. 71, pp.158-172, 2017.

[17] L. Cao, H. Li, Y. Zhang, L. Zhang, L. Xu, "Hierarchical method for cataract grading based on retinal images using improved Haar wavelet." *Information Fusion*, vol. 53, pp.196-208, 2020.

[18] J.A.A. Jothi, V.M.A.Rajam, "A survey on automated cancer diagnosis from histopathology images."*Artif Intell Rev*, vol. 48, No. 1, pp. 31–81, 2017.

[19] X. Fu, X. Cao, "Underwater image enhancement with global–local networks and compressed-histogram equalization." *Signal Processing: Image Communication*, Vol. 86, pp. 115892, 2020.

[20] Y. Fan, L. Zhang, H. Guo, H. Hao, K. Qian, "Image Processing for Laser Imaging Using Adaptive Homomorphic Filtering and Total Variation." *In Photonics*, vol. 7, no. 2, pp. 30, 2020. Multidisciplinary Digital Publishing Institute

[21] A.S. Coyner, R. Swan, J.P. Campbell, S. Ostmo, J.M. Brown, J. Kalpathy-Cramer, S.J. Kim, K.E. Jonas, R.P. Chan, M.F. Chiang, K. Sonmez, "Automated fundus image quality assessment in retinopathy of prematurity using deep convolutional neural networks." *Ophthalmology Retina*, vol. 3, No. 5, pp.444-450, 2019.

[22] R.J. Chalakkal, W.H. Abdulla, S.S. Thulaseedharan, "Quality and content analysis of fundus images using deep learning." *Computers in biology and medicine*, vol. 108, pp. 317-331, 2019.

[23] L. Abdel-Hamid, "Retinal image quality assessment using transfer learning: Spatial images vs. wavelet detail subbands." *Ain Shams Engineering Journal*, 2021.

[24] T. Pratap, P. Kokil, "Computer-aided diagnosis of cataract using deep transfer learning." *Biomedical Signal Processing and Control*, vol. 53, pp. 101533, 2019.

[25] J. Sun, C. Wan, J. Cheng, F. Yu, J. Liu, "Retinal image quality classification using fine-tuned CNN." *In Fetal, infant and ophthalmic medical image analysis*, pp. 126-133, 2017. Springer, Cham.

[26] N. Gour, P. Khanna, "Blood vessel segmentation using hybrid median filtering and morphological transformation." *In 2017 13th International Conference on Signal-Image Technology & Internet-Based Systems (SITIS)*, pp. 151-157, 2017. IEEE.

[27] M.E. Martinez-Perez, A.D. Hughes, S.A. Thom, K.H. Parker, "Improvement of a retinal blood vessel segmentation method using the Insight Segmentation and Registration Toolkit (ITK)." *In 2007 29th Annual International Conference of the IEEE Engineering in Medicine and Biology Society*, pp. 892-895, 2007. IEEE.

[28] J. Staal, M.D. Abràmoff, M. Niemeijer, M.A. Viergever, B. Van Ginneken, "Ridge-based vessel segmentation in color images of the retina." *IEEE transactions on medical imaging*, vol. 23, no. 4, pp. 501-509, 2004.

[29] J. Odstrcilik, R. Kolar, A. Budai, J. Hornegger, J. Jan, J. Gazarek, T.Kubena, P. Cernosek, O. Svoboda, E. Angelopoulou, "Retinal vessel segmentation by improved matched filtering: evaluation on a new high-resolution fundus image database." *IET Image Processing*, vol. 7, no. 4, pp.373-383, 2013.

[30] Y.Q. Zhao, X.H. Wang, X.F. Wang, F.Y. Shih, "Retinal vessels segmentation based on level set and region growing." *Pattern Recognition*, vol. 47, no. 7, pp. 2437-2446, 2014.

[31] M.G. Cinsdikici, D. Aydın, "Detection of blood vessels in ophthalmoscope images using MF/ant (matched filter/ant colony) algorithm." *Comput Methods Programs Biomed*, Vol. 96, no. 2, pp. 85e95, 2009.

[32] S. Roychowdhury, D.D. Koozekanani, K.K. Parhi, "Blood vessel segmentation of fundus images by major vessel extraction and subimage classification." *IEEE J Biomed Health Inf*, vol.19, no. 3, pp. 1118e28, 2015.

[33] M.M. Fraz, A. Basit, S.A. Barman, "Application of morphological bit planes in retinal blood vessel extraction." *J Digit Imaging*, vol. 26, no. 2, pp. 274e86, 2013.

[34] J. Dash, N. Bhoi, "A thresholding based technique to extract retinal blood vessels from fundus images." *Future Computing and Informatics Journal*, vol. 2, no. 2, pp. 103-109, 2017.

[35] A.A.G. Elseid, M.E. Elmanna, A.O. Hamza, "Evaluation of spatial filtering techniques in retinal fundus images." *American Journal of Artificial Intelligence*, vol. 2, no.2, pp.16, 2018.